

## Article

# The Heat Budget of the Tropical Pacific Mixed Layer during Two Types of El Niño Based on Reanalysis and Global Climate Model Data

Alexander Osipov \* and Daria Gushchina \* 

Department of Meteorology and Climatology, Faculty of Geography, Lomonosov Moscow State University, GSP-1, Leninskie Gory, 119991 Moscow, Russia

\* Correspondence: sashaosipov@list.ru (A.O.); dasha155@mail.ru (D.G.)

**Abstract:** The heat budget of the equatorial Pacific mixed layer during El Niño formation was studied based on reanalysis (GLORYS2V4) and model data for the modern climate. The focus of the study is on the so-called El Niño diversity, i.e., the existence of different types of events that are characterized by different locations and intensities, as well as significantly different teleconnection all around the world. The analysis of the processes that participate in the formation of different El Niño types may serve for a better understanding of the El Niño dynamic and contribute to improving its forecast. Two classifications, based on the location and intensity of the events, were considered: strong/moderate and Eastern Pacific (EP)/Central Pacific (CP). The analysis did not reveal a significant difference in the heat budget of the mixed layer between strong and EP El Niño events, as well as between moderate and CP events. The major difference in the generation mechanism of strong (EP) and moderate (CP) El Niño events consists of the magnitude of heating produced by ocean heat budget components with higher heating rates for strong (EP) events. The evolution of sea surface temperature anomalies (SSTA) is governed primarily by oceanic advection. The vertical advection (due to the thermocline feedback) is the main contributor to SSTA growth in the eastern Pacific regardless of El Niño's type. In the Central Pacific, horizontal advection is more important than vertical one, with a stronger impact of meridional processes for both strong and moderate regimes. Furthermore, the evaluation of the CMIP5 model's skill in the simulation of the processes responsible for the formation of different El Niño types was carried out. The analysis of the heat budget of the mixed layer in the CMIP5 ensemble demonstrated that the most successful models are CCSM4, CESM1-BGC, CMCC-CMS, CNRM-CM5, GFDL-ESM2M, and IPSL-CM5B-LR. They are capable of reproducing the most important contribution of the advection terms in the SSTA tendency, keeping the major role of the thermocline feedback (and vertical advection) in the eastern Pacific, and do not overestimate the contribution of zonal advective feedback. These models are recommended to be used for the analysis of El Niño mechanism modification in the future climate.

**Keywords:** El Niño–Southern Oscillation; two types of El Niño; El Niño generation mechanisms; heat budget of the ocean upper mixed layer; CMIP5 models



**Citation:** Osipov, A.; Gushchina, D. The Heat Budget of the Tropical Pacific Mixed Layer during Two Types of El Niño Based on Reanalysis and Global Climate Model Data. *Atmosphere* **2024**, *15*, 47. <https://doi.org/10.3390/atmos15010047>

Academic Editors: Shumin Chen, Weibiao Li, Yilun Chen, Aoqi Zhang and Mingsen Zhou

Received: 21 November 2023

Revised: 23 December 2023

Accepted: 27 December 2023

Published: 30 December 2023



**Copyright:** © 2023 by the authors. Licensee MDPI, Basel, Switzerland. This article is an open access article distributed under the terms and conditions of the Creative Commons Attribution (CC BY) license (<https://creativecommons.org/licenses/by/4.0/>).

## 1. Introduction

El Niño–Southern Oscillation (ENSO) is a major mode of inter-annual variability in the tropical Pacific. The global effects of ENSO, especially its warm phase (El Niño), take the form of anomalous meteorological conditions worldwide [1–5], leading to severe damage to nature and the economy of many countries. These impacts tend to be more significant during extreme El Niño events with high positive sea surface temperature anomaly (SSTA), such as very strong events of 1982–1983, 1997–1998, and 2015–2016.

For a long time, the El Niño phenomenon was considered to occur only in the eastern Pacific [6], but recently, large SST anomalies were detected in the central Pacific [7–9]. This fact highlighted the significant diversity of El Niño events and led to the definition of two

different types of ENSO: Eastern Pacific (EP) and Central Pacific (CP). According to another approach suggested by Takahashi and Dewitte [10], El Niño events are separated according to their intensity into two dynamical regimes, strong and moderate, which differ from each other not only in terms of their intensity but also have different generation mechanisms with a stronger role of atmospheric nonlinearity in the formation of strong events.

The SSTA evolution in the equatorial Pacific related to ENSO is determined by two major processes: the zonal advection and the thermocline depth fluctuations. These processes correspond to three positive types of feedback [11]: the thermocline, the zonal advective, and upwelling (Ekman pumping) feedbacks. The zonal advective feedback is associated with the advection of mean SST by anomalous zonal current ( $-u' \frac{\partial \bar{T}}{\partial x}$ ). When positive SSTA appears in the eastern equatorial Pacific, it causes the weakening of the Pacific trade winds due to reduced zonal SST gradient. Furthermore, the eastward advection of warm waters across the tropical Pacific increases and amplifies the initial warming. The upwelling feedback consists of the vertical advection of mean temperature by anomalous vertical current ( $-w' \frac{\partial \bar{T}}{\partial z}$ ). The initial SSTA causes the weakening of upwelling and thus reduces the vertical advection of cold water from the deep layers of the ocean toward the surface. The thermocline (or Ekman pumping) feedback is expressed via the vertical advection of anomalous subsurface temperature by the mean upwelling ( $-\bar{w} \frac{\partial T'}{\partial z}$ ). The thermocline deepening in response to positive SSTA results in the upward motion of warmer water, which enhances the initial warming. These positive forms of feedback may lead to a never-ending warm (or, in the case of negative initial SSTA, cold) state of the ocean–atmosphere system. So, negative feedback is needed to revert the system to a neutral state. The ocean–atmosphere net heat flux tends to dampen SSTA in response to temperature changes [11,12]. The mentioned feedbacks were shown to contribute differently to the generation of two El Niño types. The thermocline feedback plays a key role in the evolution of El Niño events with the maximum SSTA variability in the eastern Pacific, while the zonal advective feedback is responsible for SSTA growth in the central Pacific [9,13–15]. Zonal advective feedback also plays an important role in the development of strong El Niño events [16], being an important contributor to the SSTA growth both in the central and eastern Pacific [14,17]. Upwelling feedback was demonstrated to play a secondary role in the formation of both types of El Niño [9].

The analysis of the heat budget of the Pacific upper ocean mixed layer during the El Niño generation was considered in numerous studies [18–21]. This method was demonstrated to explicitly separate the contribution of different forms of feedback to the SSTA growth and therefore to reveal the dominant factor governing SSTA evolution. However, most previous studies focused on El Niño phenomena without differentiation into two types. Several studies considered the upper ocean heat budget for two types of El Niño [10,22], but only strong and moderate regimes were analyzed, while the EP/CP classification is more commonly used in the investigations of El Niño diversity. In the current studies, we used both classifications (strong/moderate and EP/CP) and compared them in terms of the El Niño formation mechanism. In order to evidence the difference in the processes responsible for SSTA generation, we not only analyzed the heat budget components during various El Niños but also made the projection of these components onto SSTA patterns in the eastern and central Pacific that allowed us to emphasize the ratio between the main ocean–atmosphere feedbacks in both regions during EP/CP and strong/moderate El Niños.

Moreover, the new reanalysis GLORYS2V4 [23] was used in the current study, which benefits from high spatial resolution, advanced bias correction scheme, and data assimilation, and thus has a strong agreement with observations. Therefore, this reanalysis may provide a more correct assessment of components of mixed layer heat budget during the generation of two types of El Niño.

Many studies highlighted that El Niño is affected by the mean state of the tropical Pacific [11,24–26]. In the context of observed global warming, it is expected that the ENSO characteristics, as well as its generation mechanism, may modify accordingly to the changes

in the mean state of the ocean–atmosphere system of the tropical Pacific. To evaluate the possible changes in the future climate, modeling studies are required. However, the state-of-the-art coupled general circulation models demonstrate a very large spread in their assessment of the ocean mixed upper layer heat budget even for the modern climate [27,28]. Moreover, the previous studies [10,22] mostly focused on the investigation of the specific models without a comparison of the model’s skill in simulating the ENSO feedbacks within the CMIP model ensemble. The current study provides the analysis of the heat budget in the model’s ensemble that aims to select the best models for further estimates of modification of the ENSO generation mechanism in future climate.

Therefore, the current investigation expands the previous research on the El Niño generation mechanism in terms of heat budget components. The novelty consists of the use of new reanalysis GLORYS2V4; in the application of two El Niño classifications (EP/CP and strong/moderate) and their comparison; and in the evaluation of CMIP model ensemble skill in simulating the heat budget of upper ocean mixed layer under El Niño conditions. The analysis of the processes that participate in the formation of different El Niño types may serve for a better understanding of the El Niño dynamic and contribute to improving its forecast. The selected models, the most successful in reproducing the upper ocean heat budget, are recommended to be used in the analysis of El Niño mechanism modification in the future climate.

The paper is organized as follows: We first describe datasets and methods used in this study (Section 2) then we assess the contribution of advective and non-advective processes to SSTA evolution for different types of El Niño based on reanalysis (Section 3.1) and models data (Section 3.2), discussing the results. Finally, we summarize the main conclusions (Section 4).

## 2. Materials and Methods

### 2.1. Data

The monthly GLORYS2V4 reanalysis (Global Ocean Reanalysis and Simulation version 4) [22] from Mercator Ocean data was used for zonal and meridional velocity components and sea water potential temperature within the upper 50 m ocean layer. This reanalysis has high-resolution horizontal ( $0.25^\circ \times 0.25^\circ$ ) and vertical (18 levels in the upper 50 m) grids. Vertical velocity was calculated using the zonal and meridional velocity components under the continuity assumption.

To estimate the ocean heat budget in the models, the historical scenario outputs of 16 global climate models from Coupled Model Intercomparison Project Phase 5 (CMIP5) were used (Table 1). The CMIP5 models were selected based on their capacity to distinguish the two ENSO regimes (Eastern Pacific and Central Pacific events) following the results obtained in [29]. We also analyzed the output of the Russian climate model INM-CM version 5.0 (Table 1). The previous version of the INM-CM model (INM-CM4) has participated in the CMIP5 phase, but following the analysis carried out in [29], it cannot explicitly separate the two types of El Niño. Therefore, we use the advanced version of this model (INM-CM5), which simulates the EP and CP El Niño rather successfully, in our study.

**Table 1.** Information on global climate models used in the study.

Model Name	Organization	City, Country	Number of Grid Cells		Number of Levels
			Longitude	Latitude	
BCC-CSM-1.1	Beijing Climate Center (BCC), China Meteorological Administration (CMA)	Beijing, China	360	232	40
CCSM4	National Center for Atmospheric Research (NCAR)	Boulder, Colorado, USA	384	320	60
CESM1-BGC					
CESM1-CAM5					

Table 1. Cont.

Model Name	Organization	City, Country	Number of Grid Cells		Number of Levels
			Longitude	Latitude	
CMCC-CESM CMCC-CM CMCC-CMS	Centro Euro-Mediterraneo sui Cambiamenti Climatici/Euro-Mediterranean Center on Climate Change (CMCC)	Lecce, Italy	182	149	31
CNRM-CM5	Centre National de Recherches Meteorologiques (CNRM), Centre Europeen de Recherche et de Formation Avanceeen Calcul Scientifique (CERFACS)	Toulouse, France	362	292	42
FIO-ESM	The First Institute of Oceanography (FIO), State Oceanic Administration (SOA)	Qingdao, China	320	384	40
GFDL-CM3 GFDL-ESM2M	National Oceanic and Atmospheric Administration (NOAA), Geophysical Fluid Dynamics Laboratory (GFDL)	Washington, D.C., USA	360	200	50
GISS-E2-H GISS-E2-R	National Aeronautics and Space Administration (NASA) Goddard Institute for Space Studies (GISS)	New York, USA	144	90	26 32
IPSL-CM5B-LR	Institut Pierre Simon Laplace (IPSL)	Guyancourt, France	182	149	31
MIROC5	Japan Agency for Marine-Earth Science and Technology	Yokosuka, Japan	256	224	50
MRI-CGCM3	Meteorological Research Institute (MRI)	Tsukuba, Japan	368	360	51
INM-CM5-0	Institute of Numerical Mathematics (INM)	Moscow, Russia	720	720	40

## 2.2. El Niño Definition

Following [30], an El Niño event was detected when the principal component (PC1) of the first EOF mode of SSTA in the tropical Pacific (10° S–10° N, 120° E–70° W) is greater than or equal to its 75 percentile over at least 5 consecutive months, regardless of the season.

ENSO diversity is characterized by the E and C indices [30], defined as follows:

$$C = \frac{PC_1 - PC_2}{\sqrt{2}}, \quad (1)$$

$$E = \frac{PC_1 + PC_2}{\sqrt{2}}, \quad (2)$$

where  $PC_1$  and  $PC_2$  are the normalized principal components of the first two EOF modes of SST anomalies in the tropical Pacific. These two indices describe major temperature variability modes of the equatorial Pacific.

The selected El Niño events were then divided into two dynamical regimes: strong and moderate following [10,31]. In the E and C indices' phase space, strong El Niño events are characterized by high positive values of the E index, while moderate events are mostly located along the C-index axis with positive values. Takahashi and Dewitte [10] showed that for observations, moderate events may be defined as those for which the E index does not exceed 1.5–1.8 °C; otherwise, the event is classified as strong. This threshold was obtained using k-mean cluster analysis [32] in the E-C phase space with  $k = 2$ , applied for the El Niño culmination phase. The threshold for the models was adapted for each model, taking into account the model SST variability.

The detected El Niño events were also classified into Eastern (EP) or Central (CP) Pacific events according to the SSTA spatial patterns. In this study, we did not use the common method based on Niño-3 and Niño-4 indices [17] that have fixed spatial coor-

dinates because, as was shown in [29], some models demonstrate a strong shift in the tropical Pacific SST variability patterns. Instead, we used the criterion based on E and C indices, which allows us to catch the area of maximum SST variability in the models. An El Niño event was defined as EP when the E value is greater than C for at least 3 consecutive months, including the event peak; when the C value is greater than the E value, an El Niño event is classified as CP. Within the EP/CP classification, we did not analyze the cases of mixed events without predominance of one of the indices.

To determine the spatial SSTA patterns associated with EP and CP events, a multiple linear regression of the SSTA onto E and C indices was applied. The E-pattern explains most of the SST variability in the eastern Pacific, and the C-pattern explains the SST variability in the central Pacific. ENSO variability is a combination of these two modes [30]. The patterns also allow us to characterize the El Niño amplitude: the E-pattern represents strong warm events, while the C-pattern corresponds to moderate warm events and cold events (La Niña) [9,33]. The E and C patterns obtained from GLORYS2V4 reanalysis are shown in Figure 1.

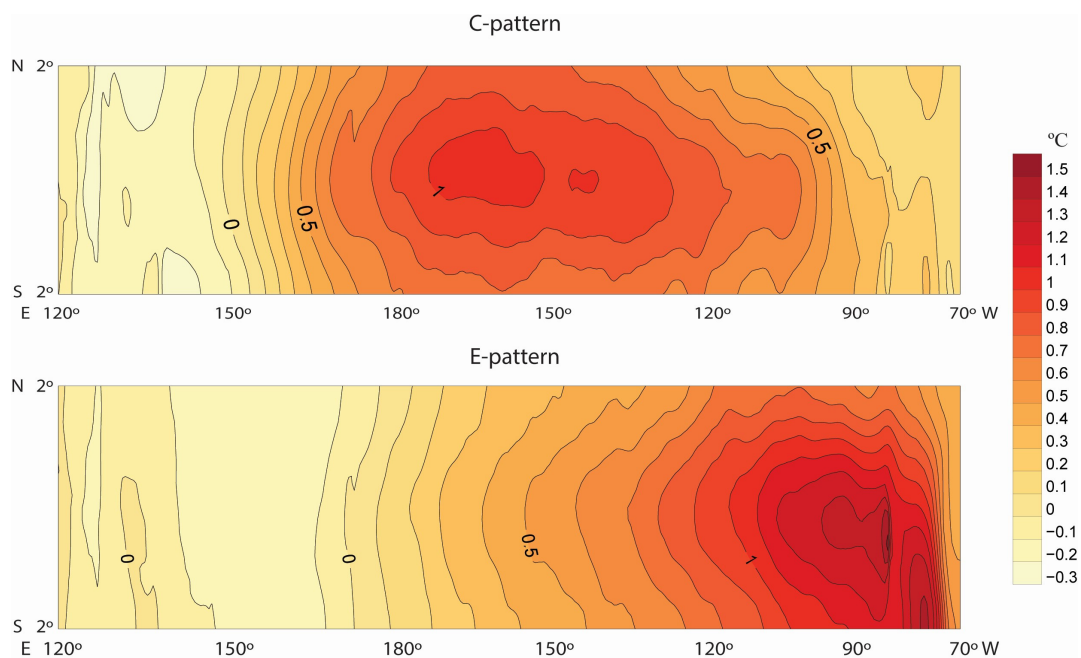


**Figure 1.** Spatial structures (patterns) of the linear regressions of the sea surface temperature anomalies onto the C and E indices associated with the moderate (C-pattern) and strong (E-pattern) El Niño regimes based on the GLORYS2V4 reanalysis data. The units are (°C).

### 2.3. The Heat Budget of the Ocean Upper Mixed Layer

To highlight the main processes contributing to ENSO-related SSTA formation, the heat budget of the upper ocean mixed layer was analyzed. A similar approach was used in a number of studies [10,14,16–19,21,34]. The fixed depth (50 m) of the mixed layer was considered to simplify calculations of the heat budget since it allows neglecting the entrainment process of heat into the mixed layer. We are motivated by previous investigations that have demonstrated the mixed layer heat budget is not sensitive to the lower depth choice [35,36], while An and Jin [19] calculated the nonlinear advection terms using both fixed and varying depth of the mixed layer, and obtained similar results. We have also compared the results obtained for two depths of the mixed layers (50 and 100 m) and revealed no significant differences (not shown).

The ocean mixed layer heat budget is formulated as follows:

$$\frac{\partial [T']}{\partial t} = \text{ADV}_{XY} + \text{ADV}_Z + \text{NDH} + Q'_{\text{net}} + R, \quad (3)$$

where  $T'$  is the temperature anomaly. The advection is separated into horizontal ( $ADV_{XY}$ ) and vertical ( $ADV_Z$ ) components:

$$ADV_{XY} \equiv \left[ -u' \frac{\partial \bar{T}}{\partial x} - v' \frac{\partial \bar{T}}{\partial y} - \bar{u} \frac{\partial T'}{\partial x} - \bar{v} \frac{\partial T'}{\partial y} \right], \quad (4)$$

$$ADV_Z \equiv \left[ -w' \frac{\partial \bar{T}}{\partial z} - \bar{w} \frac{\partial T'}{\partial z} \right], \quad (5)$$

where  $T$  is the water temperature and  $u$ ,  $v$ , and  $w$  are the horizontal, meridional, and vertical components of the velocity, respectively. Square brackets indicate vertical averaging over 50 m layer [10,18]. The over-bar represents the climatological monthly mean; the prime indicates anomalies. The non-linear dynamical heating is defined as in [10]:

$$NDH \equiv \left[ -u' \frac{\partial T'}{\partial x} - v' \frac{\partial T'}{\partial y} - w' \frac{\partial T'}{\partial z} + \overline{u' \frac{\partial T'}{\partial x}} + \overline{v' \frac{\partial T'}{\partial y}} + \overline{w' \frac{\partial T'}{\partial z}} \right], \quad (6)$$

with the seasonality of non-linear advection removed by adding the last three terms.

The term  $Q'_{net}$  corresponds to the SSTA changes produced by the net ocean–atmosphere heat fluxes anomaly, including the anomalous short-wave solar radiation, the outgoing long-wave radiation, the latent heat flux, and the sensible heat flux.  $R$  represents the residual term from the heat budget Equation (3), which includes computation errors and unresolved processes like turbulent mixing or change in temperature associated with the freshwater flux.

The climatic mean values were calculated for the period 1992–2015 for the reanalysis and 1850–2005 for the models. The linear trend was first removed from the data. To calculate spatial and temporal derivatives, we used a second-order centered-difference scheme. Therefore, when the temperature tendency is computed between the time steps  $n - 1$  and  $n + 1$ , the advective terms are calculated at the time step  $n$ .

The horizontal fields of tendency terms (horizontal and vertical advection and NDH) of the heat budget Equation (3) were then projected onto the E and C spatial patterns following [10] as (example for the E mode):

$$\left\langle \frac{\partial T'}{\partial t} \middle| E \right\rangle = \frac{1}{N_x N_y} \int_{120^\circ E}^{290^\circ E} \int_{2^\circ S}^{2^\circ N} \left( \frac{\partial T'}{\partial t}(x, y, t) \cdot E(x, y) \right) dx dy, \quad (7)$$

where  $\left\langle \frac{\partial T'}{\partial t} \middle| E \right\rangle$  is the projection of the heat budget components (horizontal and vertical advection and NDH) onto the spatial E-pattern ( $E(x, y)$ ), and  $N_x$  and  $N_y$  are the numbers of the grid points in zonal and meridional directions, respectively. This operation gives us the contribution of each heat budget component to the E and C modes, the two main modes of SST variability of the equatorial Pacific. The projections are then averaged over the equatorial Pacific ( $2^\circ S$ – $2^\circ N$ ,  $120^\circ E$ – $70^\circ W$ ). Since the method is based on the analysis of processes in the areas of maximum SST variability (obtained from EOF distribution) instead of regions with fixed coordinates (Niño-3 and Niño-4), we avoid the problem of model biases consisting in a significant shift of the SSTA maximum as compared to observations [29]. Moreover, this method allows us to compare the results obtained for modern and future climate conditions (which is the purpose of further investigation) by taking into account the possible shifts of the SST variability areas in the future climate.

To assess the differences between the various types of events, we applied composite analysis. We separately analyzed two periods corresponding to El Niño formation (generation phase) and strengthening (development phase). This approach allows us to assess the processes responsible for SSTA generation and further strengthening. In observations, the generation phase covers the period from January (0) to July (0), and the development phase lasts from July (0) to January (1); 0 denotes the year before the El Niño peak, 1—the year after the peak. In the model datasets, El Niño peaks may occur not only during the boreal winter, so we used non-fixed periods corresponding to the generation and development

phases in reanalysis: from 11 up to 5 months and 5 up to 0 months before the month of the peak, respectively.

The scheme representing the stages of the applied method is presented on Figure 2.

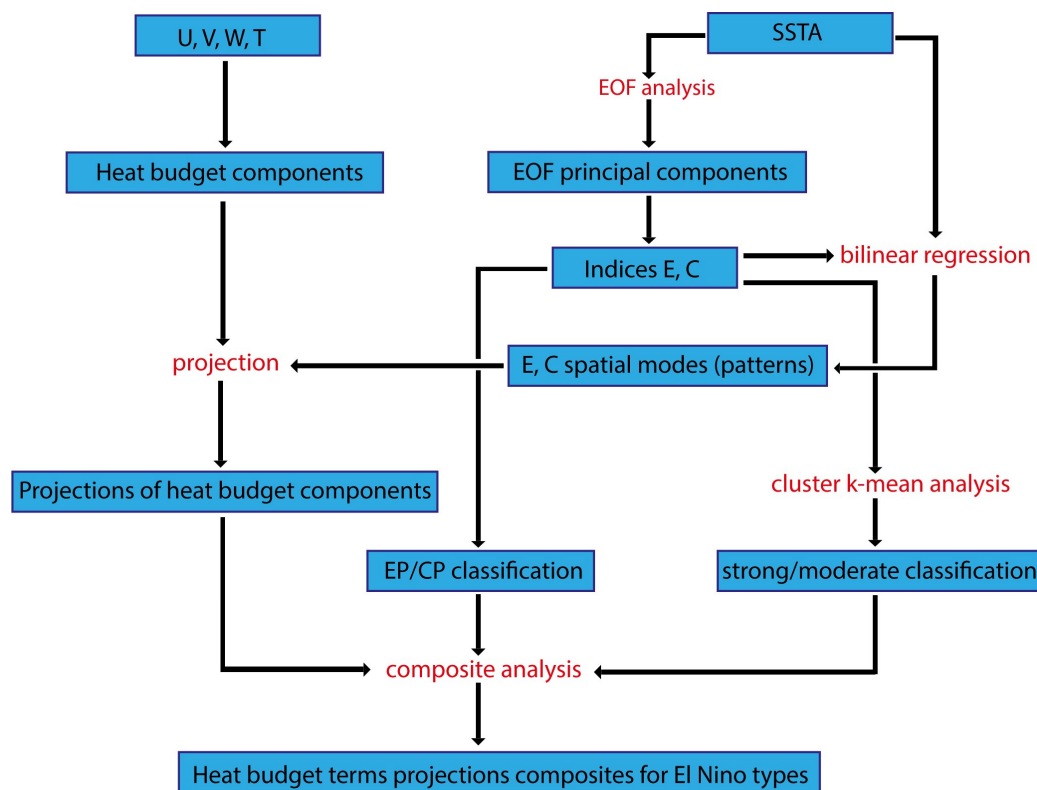


**Figure 2.** Scheme of calculation stages carried out in the study. The blue rectangles correspond to the used datasets. Red font marks the data processing operations.

### 3. Results and Discussion

#### 3.1. Observations

The analyzed period for the reanalysis (1992–2015) contains eight El Niño events, which were subdivided into types according to the two El Niño classifications (strong/moderate and EP/CP). Two El Niño events (1997–1998 and 2015–2016) are characterized by very high E index values, exceeding a threshold of 1.8 °C for the strong events (3.9 °C and 2.1 °C, respectively). On the other hand, during the El Niño event of 2009–2010 with rather high SSTA, the E index values did not reach the threshold. Therefore, two strong (1997–1998 and 2015–2016) and six moderate (1994–1995, 2002–2003, 2004–2005, 2006–2007, 2009–2010, and 2014–2015) events were defined for the analyzed period. Following the EP/CP classification, five historical El Niño events (1994–1995, 2002–2003, 2004–2005, 2009–2010, and 2014–2015) were identified as CP, and only the event of 1997–1998 was defined as EP. The events of 2006–2007 and 2015–2016 both cannot be explicitly classified as EP or CP.

Due to a rather short period covered by GLORYS2V4 reanalysis (1992–2015), we analyzed a few cases of the events of each type. The heat budget of the upper ocean mixed layer was estimated based on a longer reanalysis in [10,16,37]. However, in these studies, a different method of El Niño separation was used without projection onto E and C patterns. Therefore, in the first step, we compared the heat budget components without projections obtained from GLORYS2V4 to the results of [16,20,21,37]. It was demonstrated that the magnitude of advective terms for two historical El Niño (1997–1998 and 2015–2016) is in good agreement with those obtained in [16]. Note that in [16], the heat budget was considered for the region Niño3.4. In [21], the heat budget components were analyzed in different Niño regions. We revealed that the ratio between the ocean–atmosphere feedbacks,

as well as their temporal evolution and spatial distribution, is similar to the one obtained from GLORYS2V4 in our study, except for weaker thermocline feedback in [21]. In [20] the zonal advective feedback is the main contributor to the temperature anomaly evolution, while the role of thermocline feedback is also slightly less than in our results. The differences in the thermocline feedback magnitude may arise from the way this term is expressed in the heat budget equation or from the reanalysis biases. However, all mentioned studies show a strengthening of the thermocline feedback and a reduction in zonal advective feedback in the eastern Pacific. The study [37] states that the main SSTA growth contributors are two linear vertical feedbacks, which are followed by meridional processes and zonal advective feedback; their results as a whole agree with our findings.

As the results obtained from GLORYS2V4 are in good agreement with those obtained from longer time series, in the further analysis, we present our results based on GLORYS2V4 only but compare them to the previous findings. The GLORYS2V4 results are also used to evaluate the models.

The projections of temperature tendency terms onto E and C patterns during El Niño development, obtained from GLORYS2V4, are shown in Figure 3. Regardless of the event's type, the temperature tendency is positive during both analyzed periods (January (0)–July (0) and July (0)–January (1)). Both horizontal and vertical linear advection contribute to the SSTA growth, with the key role of vertical advection in the E-mode during the year before the El Niño peak (January (0)–January (1)), which agrees with the results of [10]. In the C-mode, the impact of horizontal and vertical advection is comparable, except for the strengthening of  $ADV_{XY}$  for the strong events. The relative importance of horizontal advection increases toward the central Pacific, where this term intensifies during the development phase (after July (0)); in the eastern Pacific,  $ADV_{XY}$ , on the contrary, weakens in the development phase (July (0)–January (1)). Nonlinear dynamic heating (advection of temperature anomalies by anomalous current) does not significantly contribute to SSTA changes, especially for the moderate events; for the strong events, this term is negative during the generation phase (January (0)–July (0)), after that NDH becomes positive. This term was shown to decrease cooling during El Niño decay [10,38]. The nonlinear advection is also a source of ENSO asymmetry, explaining stronger SSTA amplitude during warm phases [39].

The major difference between strong and moderate El Niño events consists of the magnitude of total heating rate and temperature tendency terms, which is much higher during the strong events. This difference is mostly associated with the linear advection (first of all, vertical advection— $ADV_Z$  and, to a lesser extent, horizontal advection— $ADV_{XY}$ ), which is consistent with the results of earlier studies [10,22]. Anomalous heat flux  $Q'_{net}$  provides a significant reduction in SSTA growth because of increased cloudiness over the warmer water. Therefore, this term is the main source of El Niño damping. The residual term R closes the budget, with an opposite to  $Q'_{net}$  sign.

The temperature anomalies are greater during strong events than during moderate ones and have higher SSTA growth rates during the generation phase than during the development phase. Moderate events are characterized by a more even heating tendency during the whole year before the El Niño peak.

During the strong events, the SST begins to increase earlier (in the spring of the year before the peak), and the anomalies have a longer generation period than during the moderate events (usually begin between August and October). Therefore, for some moderate events, the first period (January (0)–July (0)) does not represent the generation phase of El Niño but corresponds to the end of the previous La Niña or neutral state.

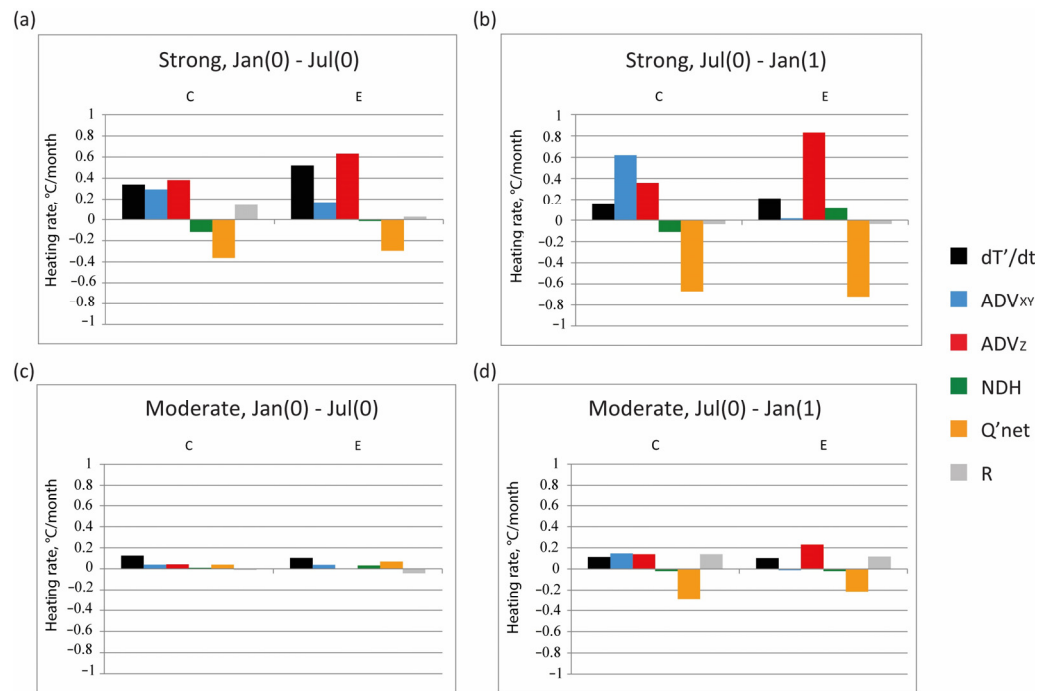


**Figure 3.** Projections of temperature tendency term and the ocean mixed layer heat budget components onto E and C patterns ( $^{\circ}\text{C}/\text{month}$ ); the composite scheme for strong (a,b) and moderate (c,d) El Niño events during generation (January (0)–July (0)) (a,c) and development phases (July (0)–January (1)) (b,d).

In the second period (July (0)–January (1)), the ratio between  $\text{ADV}_{XY}$ ,  $\text{ADV}_Z$ , and NDH remains almost the same for strong and moderate El Niño regimes except for the higher relative effect of horizontal advection in the C-mode for strong events. The residual term R has high negative values for strong El Niño events in the second period in order to counterbalance the strong advection-induced heating, while R remains positive during moderate events.

We applied the same method of heat budget analysis to another El Niño classification that is commonly used in the research considering El Niño diversity and based on the location of SSTA: EP and CP types. It was revealed that for historical El Niño events considered in the study, there is no obvious difference in the ratio between the components of the heat budget for two analyzed classifications: strong events coincide with EP type and moderate events with CP type (not shown), except for the events of 2006–2007 and 2015–2016 which were defined as mixed. Particularly, the advective terms projections for EP (CP) events are similar to those for strong (moderate), respectively. The main difference is the higher impact of zonal advective feedback on temperature evolution for EP events as compared to strong events. However, this difference is statistically insignificant because of a small number of analyzed El Niño events in observations.

Therefore, we further present the detailed analyses of the heat budget components only for strong and moderate regimes. However, the specifics of the processes in the eastern and central Pacific are taken into account via the analysis of the projections of heat budget components onto E and C patterns.

To clarify the mechanism of the contribution of vertical and horizontal advection to the formation of anomalous SST during various El Niño events, the projections of each advective term (advection of temperature by ocean currents) were analyzed to evidence the ratio between the key feedbacks during El Niño generation and development phases (Figure 4).

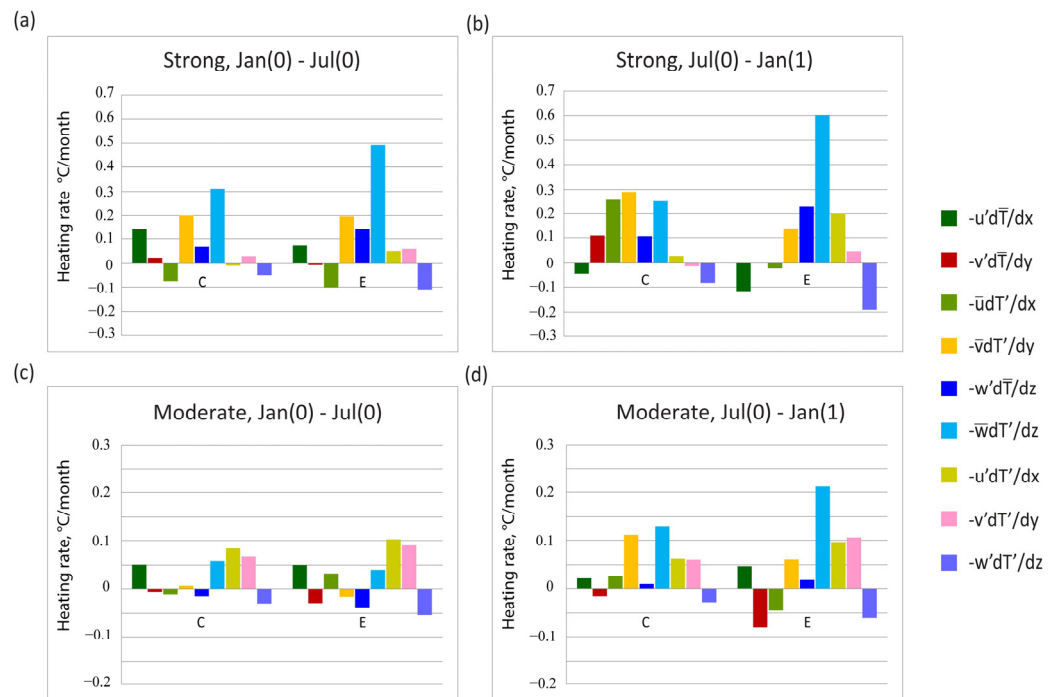


**Figure 4.** Projections of the ocean mixed layer heat budget advective components onto E and C patterns during the generation and development phases of El Niño (°C/month); the composite scheme for strong (a,b) and moderate (c,d) events during El Niño generation (January (0)–July (0) (a,c) and development phases (July (0)–January (1) (b,d)).

For strong events, the main contributor to the SSTA tendency is the term  $-\bar{w}'\frac{\partial T'}{\partial z}$  associated with the thermocline feedback; the impact of this term increases in the E-mode (Figure 4a,b), so the relative impact of the thermocline feedback increases in the eastern Pacific as the thermocline depth variations have a greater impact on the SST in this region due to a shallower thermocline [11,38]. The dominance of the thermocline feedback in the SSTA generation in the eastern Pacific is confirmed by many studies [9,11,17,22,26,40,41]. Meridional advection of temperature anomalies by the mean current  $-\bar{v}'\frac{\partial T'}{\partial y}$  also plays an important role in SSTA growth, especially in C-mode. This anomalous advection corresponds to the recharge of the heat toward the equator, which plays an important role in the ENSO dynamics as formulated in the recharge–discharge theory [42]. Another vertical term  $-w'\frac{\partial \bar{T}}{\partial z}$  associated with the upwelling feedback also plays an important role with a higher contribution into E-mode. The term  $-u'\frac{\partial \bar{T}}{\partial x}$  associated with zonal advective feedback contributes to the temperature growth only in the El Niño generation phase. In contrast, during the development phase, this term tends to reduce the heating rate. Zonal advection of anomalous temperature by the mean current  $\bar{u}'\frac{\partial T'}{\partial x}$  plays an important role in C-mode during the El Niño development phase. The term  $-w'\frac{\partial T'}{\partial z}$ , corresponding to the nonlinear vertical advection, was demonstrated to contribute mostly to El Niño damping, consistent with [43].

As for moderate events (Figure 4c,d), the magnitude of advective term projections is smaller than for the strong ones. The thermocline feedback ( $-\bar{w}'\frac{\partial T'}{\partial z}$ ) plays an important role during El Niño enhancement (July (0)–January (1)) with a higher contribution to the E-mode. Meridional advection of anomalous heat  $-\bar{v}'\frac{\partial T'}{\partial y}$  also represents a significant source of temperature growth, but only during the development phase (July (0)–January (1)). Zonal advective feedback stays positive during the development phase of El Niño in contrast to the strong events. Upwelling feedback is a minor contributor to the heating process. Non-linear horizontal advection terms  $-u'\frac{\partial T'}{\partial x}$ ,  $-v'\frac{\partial T'}{\partial y}$  also play a significant role during moderate events generation phase.

We have compared our results obtained from GLORYS2V4 reanalysis with the ones of Takahashi and Dewitte [10], who calculated projections onto the E index for strong and moderate El Niño using the Drakkar data. Our results are similar to their estimates in terms of the ratio between the heat budget terms and their dynamics (enhancement of vertical advection and weakening of horizontal advection in the second period). However, our heating terms have a higher magnitude due to fewer cases of analyzed events that are classified as extreme El Niños (1997–1998 and 2015–2016).

In summary, strong (EP) and moderate (CP) El Niño events differ from each other mainly in the heating rate and the development phase duration, as moderate events tend to begin later. Vertical advection plays a key role in the Eastern Pacific (E-mode) predominantly due to the thermocline feedback, regardless of the El Niño type. In the Central Pacific (C-mode), horizontal advection becomes more important, with a strong impact on meridional processes, for both strong and moderate regimes.

### 3.2. Models

As mentioned in the previous section, the number of El Niño events in observations is rather limited, which complicates the analysis of the difference between the El Niño types due to a small number of events of each type. To resolve this problem, the analysis of long model runs containing a larger number of the events is commonly used (e.g., [22,29]). In the current research, we analyze the simulation of the ocean mixed layer heat budget in the ensemble consisting of 16 CMIP5 models and the INM-CM5 model (see Section 2). At first, we detected El Niño events in the models using PC1 value (see Section 2). In this step, we considered all El Niño events regardless of the peak timing (in reanalysis, the peak usually occurs in boreal winter). The number of El Niño events over the analyzed period (155 years) varies significantly among the models (Table 2). In the second step, we excluded from the analysis the events without a clear peak or with a peak occurring in boreal summer because these events may be associated with some unrealistic interactions between SSTA dynamics and the seasonal cycle. We also did not analyze the weak events in case of their development in the year following strong El Niño as it is difficult to separate the processes of decaying of the previous event and development of the new event.

To separate the selected events into strong and moderate types, we performed k-mean clustering within each model dataset using peak values of the E-index. The threshold separating two clusters varies among the models in a wide range from 1.5 °C to 3.3 °C (Table 2). Only half of the models demonstrate the bimodal distribution of the El Niño peaks in E-C phase space. The events that cannot be definitely classified as strong or moderate (mostly the events with E-index close to the threshold) were excluded from further analysis. The analysis of Table 2 demonstrates that all models generated more moderate than strong events, except for GFDL-ESM2M.

The classification into EP and CP types was based on the predominance of the E/C index during the El Niño peak. The ratio between these two types also varies significantly among the models (Table 2), but the majority of the models tend to reproduce more EP events.

Furthermore, the composites of the upper ocean layer heat budget components were calculated for strong and moderate EP/CP events in the models and compared to the reanalysis. Two periods—El Niño generation and development phases—were considered analogically to the reanalysis. However, the periods were not fixed in calendar months as model peaks of El Niño may occur in various months (not obligatory in December–January as in reanalysis). Therefore, we defined two periods as follows: the generation phase contains the months from 11 up to 5 before the peak of the event (corresponding to the period January (0) to July (0) in reanalysis), and the development phase contains the months from 5 up to 0 before the peak (correspond to the period July (0) to January (1) in reanalysis).

**Table 2.** Number of identified El Niño events (total and for each type of El Niño) and strong El Niño threshold values for the analyzed models.

Model Name	Total Number	Events Selected	Strong	Moderate	EP	CP	E-Index Threshold Values, °C
BCC-CSM1-1	51	40	7	16	13	6	1.6–1.7
CCSM4	42	42	7	30	12	14	2.6–2.8
CESM1-BGC	41	38	7	17	11	10	1.8–2.3
CESM1-CAM5	46	45	7	33	13	12	2.0–2.2
CMCC-CESM	38	35	4	21	9	9	2.0
CMCC-CM	39	35	3	21	12	3	2.7–3.3
CMCC-CMS	44	40	3	23	8	7	2.2–2.5
CNRM-CM5	50	48	4	37	9	11	2.1–2.2
FIO-ESM	46	43	5	18	13	9	1.9
GFDL-CM3	45	42	9	25	11	7	1.7–2.0
GFDL-ESM2M	36	36	11	13	12	12	1.5–2.1
GISS-E2-H	46	42	5	25	8	7	1.6–1.8
GISS-E2-R	45	40	7	19	19	7	1.5–2.2
IPSL-CM5B-LR	42	35	10	17	17	8	1.6–2.0
MIROC5	33	30	3	21	7	12	1.7–2.7
MRI-CGCM3	45	41	3	25	15	9	1.7–2.0
INM-CM5-0	39	34	3	20	9	6	2.0–2.7

In Figure 5, the components of the heat budget equation are presented (for all El Niño events without separation into types). For all models, the main contributors to the SSTA growth are the advection terms, except for MIROC5, where zonal advection leads to the SSTA reduction (negative term) and is compensated by unrealistic heating related to NDH (Figure 5). We revealed that these biases in MIROC5 are related to strong negative  $-v'\frac{\partial T}{\partial y}$  term in the meridional advection and strong positive  $-w'\frac{\partial T}{\partial y}$  term in NDH (not shown). Thus, we suppose that MIROC5 cannot reproduce the ocean dynamics during El Niño development correctly and excluded this model from further analysis.

As a second step of model validation, we analyzed the projection of tendency terms onto the E and C patterns separately for strong and moderate events during two periods—generation and development phases (Figure 6) and compared these projections with the ones obtained from reanalysis. About half of the models underestimate the contribution of the vertical advection to the total SSTA growth. The term  $ADV_z$  in reanalysis provides the major SSTA growth in the E-mode (Figure 6) and remains significant in the C-mode. The models BCC-CSM1-1, CESM1-CAM5, CMCC-CESM, GISS-E2-H, and GISS-E2-R do not reproduce the dominant contribution of the vertical advection to the E-mode, especially for strong El Niño events. Some models (FIO-ESM, GFDL-CM3, INM-CM5-0, and MRI-CGCM3) underestimate the role of  $ADV_z$  in the total heating rate. Only five models (CESM1-BGC, CMCC-CM, CNRM-CM5, GFDL-ESM2M, and IPSL-CM5B-LR) simulate the main contribution of  $ADV_z$  to the total heating as in reanalysis.

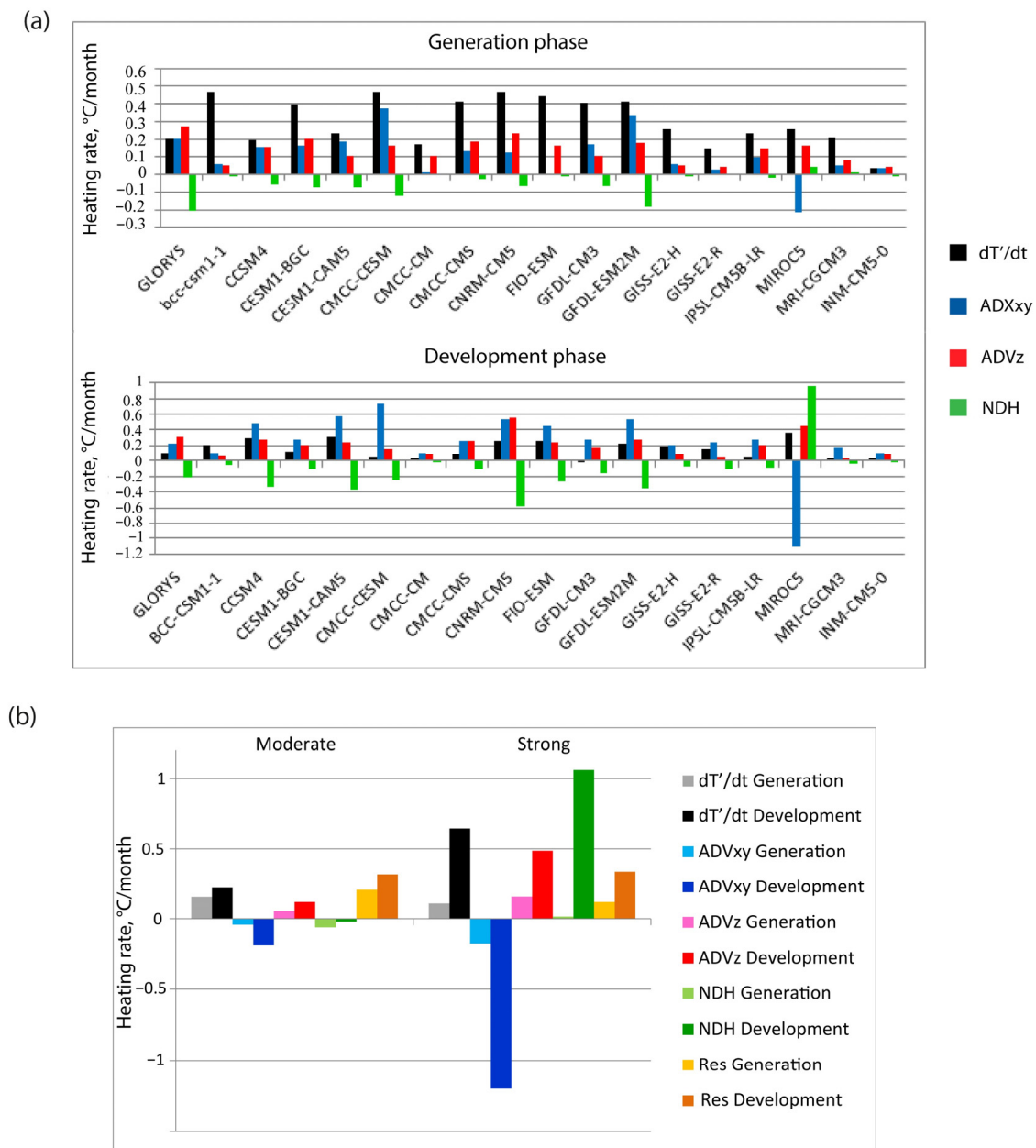


**Figure 5.** (a) Heat budget tendency terms (°C/month) during El Niño generation (top panel) and development (bottom panel) phases for reanalysis and models; (b) composites of tendency terms for strong and moderate El Niño events for MIROC5 during generation and development phases.

As for zonal advection, only BCC-CSM1-1 fails to reproduce the heating provided by this term; two more models (GISS-E2-H and GISS-E2-R) simulate negative  $ADV_{xy}$  during El Niño generation phase, but this term becomes positive during the development phase. The other 13 models agree with the reanalysis in the simulation of the SSTA growth due to zonal advection. All analyzed models reproduce the damping effect of NDH, but three of them (BCC-CSM1-1, INM-CM5-0, and MRI-CGCM3) demonstrate too weak cooling due to this term as compared to reanalysis.

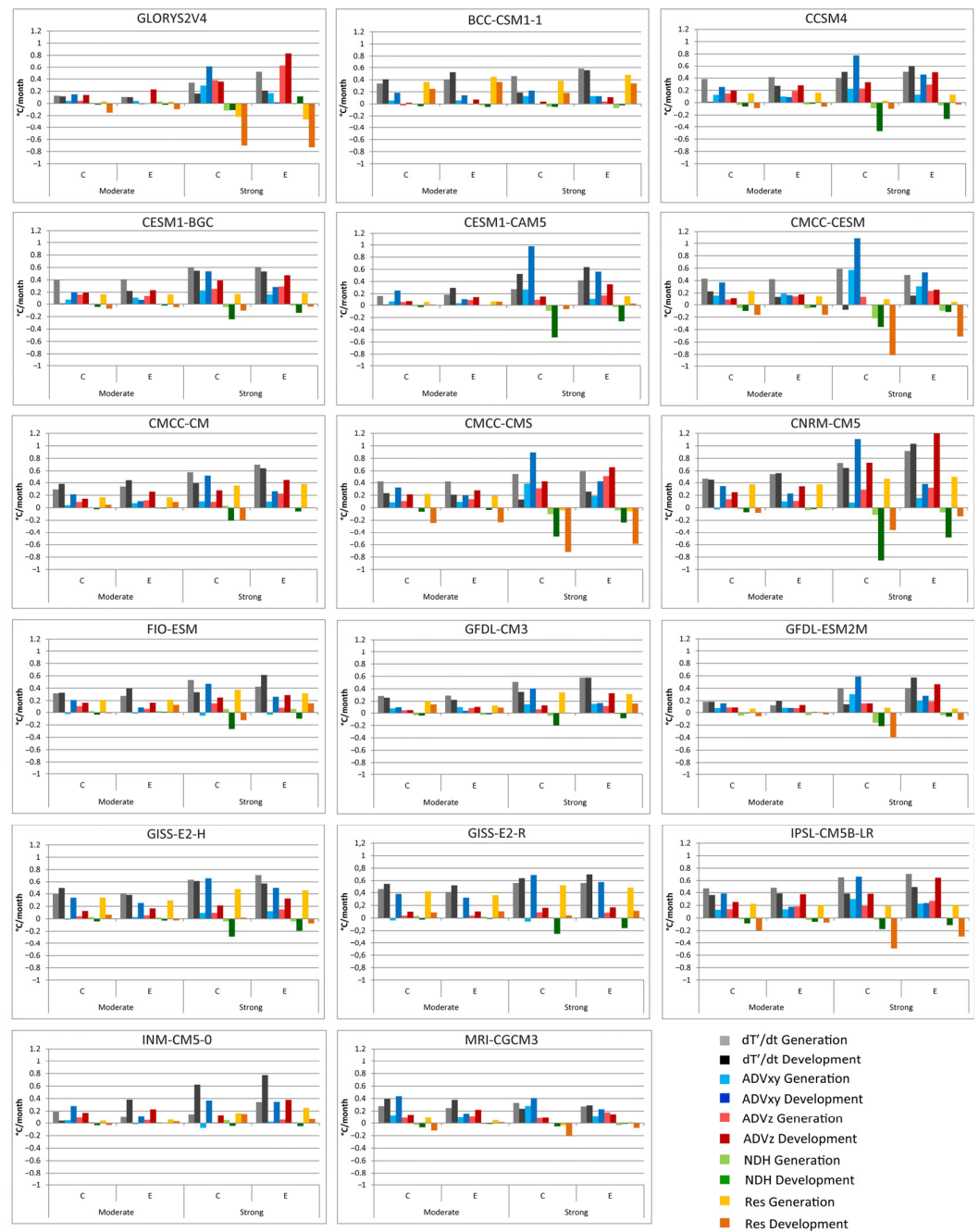


**Figure 6.** Projections of temperature tendency and the ocean mixed layer heat budget components onto E and C patterns ( $^{\circ}\text{C}/\text{month}$ ) for reanalysis and models; the composite scheme for moderate and strong El Niño events during generation (January (0)–July (0)) and development (July (0)–January (1)) phases.

Several models significantly underestimate the heating induced by advection, both horizontal and vertical. BCC-CSM1-1 reproduces very high positive values of the residual term Res relative to reanalysis. It should be noted that for the models, we considered the residual term as a sum of net surface heat flux  $Q'_{\text{net}}$  and the residual term R from Equation (3). We revealed that in reanalysis, the large  $Q'_{\text{net}}$  values tend to be balanced by high R values with the opposite sign (Figure 3), while the major heating tendency is provided by the advection. Therefore, we did not separate  $Q'_{\text{net}}$  and R in the model analysis, focusing on the correct simulation of advection terms. As mentioned above, BCC-CSM1-1 simulates a much smaller magnitude of advective tendency terms than Res. It thus produces the El Niño related warming due to non-advective factors likely associated with the strong

contribution of the radiative heating to the SSTA growth. Unresolved processes in the mixed layer are another possible source of high Res values. Several models (CMCC-CM, FIO-ESM, GFDL-CM3, GISS-E2-H, GISS-E2-R, and INM-CM5-0) also overestimate the heating effect provided by the residual term and reproduce insufficient advective heating, but all these models show higher relative impact of advective processes to the El Niño generation as compared to BCC-CSM1-1.

In reanalysis, the heating provided by advection exceeds the total SSTA growth during El Niño development and is compensated by high negative values of the residual term Res that closes the heat budget. Only a few models (CMCC-CESM, CMCC-CMS, GFDL-ESM2M, IPSL-CM5B-LR, and, to a lesser extent, MRI-CGCM3) reproduce the SSTA damping by negative Res values, as in observations. CCSM4, CESM1-BGC, CESM1-CAM5, and CNRM-CM5 also demonstrate heating due to advection stronger than the total heating rate, although the compensating damping in these models is provided by NDH, while Res does not significantly decrease the SSTA. All mentioned models, however, correctly reproduce the advection as a key factor of SSTA growth.

We analyzed two classifications of El Niño: strong/moderate regimes and EP/CP events. However, our analysis did not reveal significant differences in the upper ocean heat budget between strong and EP events, as well as between moderate and CP events in the considered models. Therefore, we did not present the composite schemes for the EP/CP classification.

We have also examined the contribution of the key feedbacks to the SSTA evolution in the models. In observations, the thermocline feedback provides the strongest heating effect with the maximum contribution in the eastern Pacific (see Figure 4). All models, except for BCC-CSM1-1, GISS-E2-R, and INM-CM5-0, reproduce this feature (not shown). The upwelling feedback is adequately simulated by the analyzed models, although BCC-CSM1-1 and INM-CM5-0 make this feedback the main contributor to the  $ADV_Z$  term instead of the thermocline feedback. This is due to vertical heat advection in these models being primarily related to the weakening of upwelling, while the thermocline deepening is not reproduced correctly and has a rather small impact on the SSTA evolution. The zonal advective feedback provides SSTA growth in all models, but the contribution of this feedback to the El Niño total heating is higher than in the reanalysis. Two models fail to reproduce the zonal advective feedback correctly: in INM-CM5-0 contribution of this term is too weak, while in GISS-E2-R, it is overestimated.

The correct ratio between the thermocline feedback and the zonal advective feedback in the generation of SSTA during El Niño is simulated by two models of the ensemble: CESM1-BGC and IPSL-CM5B-LR. The term  $-\bar{v} \frac{\partial T'}{\partial y}$  representing the heat recharge toward the equator is reproduced by all analyzed models.

The SSTA decrease in the reanalysis is mainly provided by the nonlinear vertical advection  $-w' \frac{\partial T'}{\partial z}$ . However, in a majority of the models, the damping occurs via nonlinear horizontal advection, especially in the C-mode. About half of the models simulate the cooling effect due to  $-w' \frac{\partial T'}{\partial z}$ , but only in IPSL-CM5B-LR, MRI-CGCM3 this term is the main source of SSTA reduction.

Thus, after the heat budget terms assessment, we selected six models that reproduce processes within the ocean's upper mixed layer during El Niño generation and development in the most appropriate way. These models are CCSM4, CESM1-BGC, CMCC-CMS, CNRM-CM5, GFDL-ESM2M, and IPSL-CM5B-LR.

#### 4. Conclusions

The ocean mixed layer heat budget was analyzed to understand the role of the main ocean–atmosphere feedbacks in the El Niño generation mechanism based on the GLO-RYS2V4 reanalysis and compared to the results of previous studies based on longer ocean reanalysis. The ensemble of 16 CMIP5 models and the INM-CM5 model was evaluated in order to assess the model's skill in reproducing the ocean mixed layer heat budget during El Niño generation.

The El Niño diversity was taken into account accordingly to two classifications: strong/moderate regimes and Eastern/Central Pacific types of the events, and the comparison of these classifications was carried out. The analysis did not reveal the significant differences in the generation mechanism between strong and EP events, as well as between moderate and CP events both in reanalysis and models.

The major difference between the two types of El Niño consists of the higher magnitude of total heating rate and temperature tendency terms for the strong El Niño events as compared to moderate, whereas more intense advective heating generates a stronger SSTA. The total heating rate is higher in the first half of the year before the peak of strong El Niños, while during the moderate events, it is more even for the generation and development phases.

Both for strong and moderate events, advection ensures the SSTA rise in E and C modes. The vertical advection plays a key role in the SSTA growth in the eastern Pacific regardless of the event's type, primarily due to the contribution of the thermocline feedback. Upwelling feedback is important for the generation of strong events, while for moderate events, it plays a minor role. The horizontal advection becomes significant in the central Pacific for the strong events, with more effective heating produced by meridional advection of temperature anomalies, while zonal processes play a secondary role. Zonal advective feedback provides heating only during the generation phase of strong El Niño events, while for moderate events, this feedback stays positive up to the peak. Nonlinear dynamic heating contributes to the ocean cooling in the central Pacific, while it leads to the heating in the Eastern Pacific during the development phase of strong El Niño events. For moderate El Niños, NDH does not play a significant role in the evolution of the SSTA. The surface heat fluxes mostly provide the SSTA damping, although they are balanced by other unresolved processes.

The main limitation of the current study is associated with a rather short period covered by the used reanalysis that results in a small number of the El Niño events of each type that were included in the composites. Partially, this limitation was compensated by the comparison of heat budget components obtained from GLORYS2V4 with previous results based on longer reanalysis with a larger number of El Niño events. The comparison demonstrated good agreement between our results and previous results in terms of the ratio between the heat budget terms and their dynamics.

Noteworthy, in current research, for the first time, the two different classifications of El Niño were considered, while the projections of the heat budget components onto E and C patterns allowed to specify the SSTA generation mechanism in the eastern and central Pacific.

One of the main purposes of the study was to evaluate the skill of an ensemble of 16 CMIP5 and INM-CM5 models in reproducing the evolution of the ocean mixed layer heat budget during the El Niño generation with a focus on the relative contribution of the main ocean–atmosphere feedbacks into the SSTA growth. We found that most of the analyzed models tend to correctly reproduce the main processes in the ocean mixed layer responsible for the generation of SSTA in the equatorial Pacific during El Niño, although they are not always successful in the simulation of the ratio between the main feedbacks. The best models are those that reproduce the most important contribution of the advection terms in the SSTA tendency, keep the major role of the thermocline feedback (and vertical advection) in the eastern Pacific, and do not overestimate the contribution of zonal advective feedback. Thus, we selected 6 CMIP5 models that are able to reproduce the mechanisms of SSTA formation during El Niño with the differentiation of the processes involved in the generation of strong and moderate regimes: CCSM4, CESM1-BGC, CMCC-CMS, CNRM-CM5, GFDL-ESM2M, and IPSL-CM5B-LR. These models are suitable for further investigations of El Niño mechanism changes in future climate.

The findings of the study may contribute to a better understanding of the El Niño diversity in terms of the processes governing its generation and may be useful to identify the type of developing event relying on the contribution of various feedbacks. The evaluation of the model's skill in reproducing these processes carried out for the first time in the current investigation for the model ensemble, provides a useful tool for further investigation of the modification of the El Niño associated ocean heat budget anomalies in the future

climate. Another prospective research direction consists of the evaluation of the next model's generation (CMIP6 phase), which will probably increase the number of the models capable of accurately simulating the heat budget components and is therefore suitable for estimating El Niño modification in future climate events.

**Author Contributions:** Conceptualization, A.O. and D.G.; methodology, A.O. and D.G.; software, A.O.; validation, A.O. and D.G.; formal analysis, A.O.; investigation, A.O. and D.G.; resources, A.O.; data curation, A.O.; writing—original draft preparation, A.O.; writing—review and editing, A.O. and D.G.; visualization, A.O.; supervision, A.O. and D.G.; project administration, D.G.; funding acquisition, D.G. All authors have read and agreed to the published version of the manuscript.

**Funding:** This research was funded by the Russian Science Foundation, grant number 20-17-00190.

**Institutional Review Board Statement:** Not applicable.

**Informed Consent Statement:** Not applicable.

**Data Availability Statement:** Publicly available datasets were analyzed in this study. This data can be found here: <http://marine.copernicus.eu/services-portfolio/access-to-products/> (accessed on 21 November 2023).

**Acknowledgments:** The authors thank Boris Dewitte for providing the GLORYS2V4 data, for computational assistance, and for fruitful and constructive discussion during the preparation of the manuscript.

**Conflicts of Interest:** The authors declare no conflicts of interest.

## References

- Ropelewski, C.F.; Halpert, M.S. Global and Regional Scale Precipitation Patterns Associated with the El Niño/Southern Oscillation. *Mon. Weather Rev.* **1987**, *115*, 1606–1626. [[CrossRef](#)]
- Trenberth, K.E.; Branstator, W.B.; Karoly, D.; Kumar, A.; Lau, N.C.; Ropelewski, C.F. Progress during TOGA in understanding and modeling global teleconnections associated with tropical sea surface temperatures. *J. Geophys. Res.* **1998**, *103*, 14291–14324. [[CrossRef](#)]
- Yeh, S.-W.; Cai, W.; Min, S.-K.; McPhaden, M.J.; Dommenges, D.; Dewitte, B.; Collins, M.; Ashok, K.; An, S.; Yim, B.; et al. ENSO atmospheric teleconnections and their response to greenhouse gas forcing. *Rev. Geophys.* **2018**, *56*, 185–206. [[CrossRef](#)]
- McPhaden, M.J.; Zebiak, S.E.; Glantz, M.H. ENSO as an integrating concept in earth science. *Science* **2006**, *314*, 1740–1745. [[CrossRef](#)]
- Cai, W.; Santoso, A.; Collins, M.; Dewitte, B.; Karamperidou, C.; Kug, J.-S.; Lengaigne, M.; McPhaden, M.J.; Stuecker, M.F.; Taschetto, A.S.; et al. Changing El Niño–Southern Oscillation in a warming climate. *Nat. Rev. Earth Environ.* **2021**, *2*, 628–644. [[CrossRef](#)]
- Rasmusson, E.M.; Carpenter, T.H. Variations in Tropical Sea Surface Temperature and Surface Wind Fields Associated with the Southern Oscillation/El Niño. *Mon. Wea. Rev.* **1982**, *110*, 354–384. [[CrossRef](#)]
- Ashok, K.; Behera, S.K.; Rao, S.A.; Weng, H.; Yamagata, T. El Niño Modoki and its possible teleconnection. *J. Geophys. Res.* **2007**, *112*, C11007. [[CrossRef](#)]
- Kao, H.-Y.; Yu, J.-Y. Contrasting Eastern-Pacific and Central-Pacific Types of ENSO. *J. Clim.* **2009**, *22*, 615–632. [[CrossRef](#)]
- Kug, J.S.; Jin, F.F.; An, S.I. Two types of El Niño events: Cold tongue El Niño and warm pool El Niño. *J. Clim.* **2009**, *22*, 1499–1515. [[CrossRef](#)]
- Takahashi, K.; Dewitte, B. Strong and moderate nonlinear El Niño regimes. *Clim. Dyn.* **2016**, *46*, 1627–1645. [[CrossRef](#)]
- Jin, F.-F.; Kim, S.T.; Bejarano, L. A coupled-stability index for ENSO. *Geophys. Res. Lett.* **2006**, *33*, L23708. [[CrossRef](#)]
- Zebiak, S.E.; Cane, M.A. A model El Niño–Southern Oscillation. *Mon. Wea. Rev.* **1987**, *115*, 2262–2278. [[CrossRef](#)]
- Choi, J.; An, S.-I.; Kug, J.-S.; Yeh, S.-W. The role of mean state on changes in El Niño's flavor. *Clim. Dyn.* **2011**, *37*, 1205–1215. [[CrossRef](#)]
- Capotondi, A. ENSO diversity in the NCAR CCSM4 climate model. *J. Geophys. Res. Oceans* **2013**, *118*, 4755–4770. [[CrossRef](#)]
- Ren, H.-L.; Jin, F.-F. Recharge Oscillator Mechanisms in Two Types of ENSO. *J. Clim.* **2013**, *26*, 6506–6523. [[CrossRef](#)]
- Abellán, E.; McGregor, S.; England, M.H.; Santoso, A. Distinctive role of ocean advection anomalies in the development of the extreme 2015–2016 El Niño. *Clim. Dyn.* **2017**, *51*, 2191–2208. [[CrossRef](#)]
- Kug, J.S.; Choi, J.; An, S.-I.; Jin, F.-F.; Wittenberg, A.T. Warm pool and cold tongue El Niño events as simulated by the GFDL 2.1 coupled GCM. *J. Clim.* **2010**, *23*, 1226–1239. [[CrossRef](#)]
- Jin, F.-F.; An, S.-I.; Timmermann, A.; Zhao, J. Strong El Niño events and nonlinear dynamical heating. *Geophys. Res. Lett.* **2003**, *30*, 1120. [[CrossRef](#)]
- An, S.-I.; Jin, F.-F. Nonlinearity and Asymmetry of ENSO. *J. Clim.* **2004**, *17*, 2399–2412. [[CrossRef](#)]

20. Kim, W.; Cai, W.; Kug, J.-S. Migration of atmospheric convection coupled with ocean currents pushes El Niño to extremes. *Geophys. Res. Lett.* **2015**, *42*, 3583–3590. [[CrossRef](#)]
21. Santoso, A.; McPhaden, M.J.; Cai, W. The Defining Characteristics of ENSO Extremes and the Strong 2015/2016 El Niño. *Rev. Geophys.* **2017**, *55*, 1079–1129. [[CrossRef](#)]
22. Carréric, A.; Dewitte, B.; Cai, W.; Capotondi, A.; Takahashi, K.; Yeh, S.-W.; Wang, G.; Guémas, V. Change in strong Eastern Pacific El Niño events dynamics in the warming climate. *Clim. Dyn.* **2020**, *54*, 901–918. [[CrossRef](#)]
23. Garric, G.; Parent, L.; Greiner, E.; Drévilion, M.; Hamon, M.; Lellouche, J.M.; Régnier, C.; Desportes, C.; Le Galloudec, O.; Bricaud, C.; et al. Performance and quality assessment of the global ocean eddy-permitting physical reanalysis GLORYS2V4. In Proceedings of the EGU General Assembly, Vienna, Austria, 23–28 April 2017; Volume 19, p. 18776.
24. Fedorov, A.V.; Philander, S.G. Is El Niño Changing? *Science* **2000**, *288*, 1997–2002. [[CrossRef](#)]
25. DiNezio, P.N.; Kirtman, B.P.; Clement, A.C.; Lee, S.-K.; Vecchi, G.A.; Wittenberg, A. Mean Climate Controls on the Simulated Response of ENSO to Increasing Greenhouse Gases. *J. Clim.* **2012**, *25*, 7399–7420. [[CrossRef](#)]
26. Fedorov, A.V.; Hu, S.; Lengaigne, M.; Guilyardi, E. The impact of westerly wind bursts and ocean initial state on the development, and diversity of El Niño events. *Clim. Dyn.* **2015**, *44*, 1381–1401. [[CrossRef](#)]
27. Kim, S.T.; Cai, W.; Jin, F.-F.; Yu, J.-Y. ENSO stability in coupled climate models and its association with mean state. *Clim. Dyn.* **2014**, *42*, 3313–3321. [[CrossRef](#)]
28. Karamperidou, C.; Jin, F.-F.; Conroy, J.L. The importance of ENSO nonlinearities in tropical pacific response to external forcing. *Clim. Dyn.* **2017**, *49*, 2695–2704. [[CrossRef](#)]
29. Cai, W.; Wang, G.; Dewitte, B.; Lixin, W.; Santoso, A.; Takahashi, K.; Yang, Y.; Carréric, A.; McPhaden, M.J. Increased variability of Eastern Pacific El Niño under greenhouse warming. *Nature* **2018**, *564*, 201–206. [[CrossRef](#)]
30. Takahashi, K.; Montecinos, A.; Goubanova, K.; Dewitte, B. ENSO regimes: Reinterpreting the canonical and Modoki El Niño. *Geophys. Res. Lett.* **2011**, *38*, L10704. [[CrossRef](#)]
31. Takahashi, K.; Karamperidou, C.; Dewitte, B. A theoretical model of strong and moderate El Niño regimes. *Clim. Dyn.* **2018**, *52*, 7477–7493. [[CrossRef](#)]
32. Hartigan, J.A.; Wong, M.A. Algorithm AS 136: A K-Means Clustering Algorithm. *J. R. Stat. Soc. Ser. C Appl. Stat.* **1979**, *28*, 100–108. [[CrossRef](#)]
33. Dewitte, B.; Takahashi, K. Diversity of moderate El Niño events evolution: Role of air–sea interactions in the eastern tropical Pacific. *Clim. Dyn.* **2017**, *52*, 7455–7476. [[CrossRef](#)]
34. Wang, G.; Cai, W.; Santoso, A. Stronger Increase in the Frequency of Extreme Convective than Extreme Warm El Niño Events under Greenhouse Warming. *J. Clim.* **2019**, *33*, 675–690. [[CrossRef](#)]
35. Feng, M.; Hacker, P.; Lukas, R. Upper ocean heat and salt balances in response to a westerly wind burst in the western equatorial Pacific during TOGA COARE. *J. Geophys. Res. Oceans* **1998**, *103*, 10289–10311. [[CrossRef](#)]
36. Wang, B.; Luo, X.; Sun, W.; Yang, Y.-M.; Liu, J. El Niño diversity across boreal spring predictability barrier. *Geophys. Res. Lett.* **2020**, *47*, e2020GL087354. [[CrossRef](#)]
37. Pan, X.; Li, T.; Chen, M. Change of El Niño and La Niña amplitude asymmetry around 1980. *Clim Dyn.* **2020**, *54*, 1351–1366. [[CrossRef](#)]
38. An, S.-I.; Jin, F.-F. Collective Role of Thermocline and Zonal Advective Feedbacks in the ENSO Mode. *J. Clim.* **2001**, *14*, 3421–3432. [[CrossRef](#)]
39. Yu, J.; Li, T.; Jiang, L. Why Does a Stronger El Niño Favor Developing towards the Eastern Pacific while a Stronger La Niña Favors Developing towards the Central Pacific? *Atmosphere* **2023**, *14*, 1185. [[CrossRef](#)]
40. Neelin, J.D.; Battisti, D.S.; Hirst, A.C.; Jin, F.-F.; Wakata, Y.; Yamagata, T.; Zebiak, S.E. ENSO theory. *J. Geophys. Res. Oceans* **1998**, *103*, 14261–14290. [[CrossRef](#)]
41. Borlace, S.; Cai, W.; Santoso, A. Multidecadal ENSO amplitude variability in a 1000-yr simulation of a coupled global climate model: Implications for observed ENSO variability. *J. Clim.* **2013**, *26*, 9399–9407. [[CrossRef](#)]
42. Jin, F.-F. An Equatorial Ocean Recharge Paradigm for ENSO. Part I: Conceptual Model. *J. Atmos. Sci.* **1997**, *54*, 811–829. [[CrossRef](#)]
43. Su, J.; Zhang, R.; Li, T.; Rong, X.; Kug, J.-S.; Hong, C.-C. Causes of the El Niño and La Niña amplitude asymmetry in the equatorial eastern Pacific. *J. Clim.* **2010**, *23*, 605–617. [[CrossRef](#)]

**Disclaimer/Publisher’s Note:** The statements, opinions and data contained in all publications are solely those of the individual author(s) and contributor(s) and not of MDPI and/or the editor(s). MDPI and/or the editor(s) disclaim responsibility for any injury to people or property resulting from any ideas, methods, instructions or products referred to in the content.